Accepted manuscript doi:
10.1680/jgele.18.00230

Submitted: 07 December 2018

Published online in 'accepted manuscript' format: 27 August 2019

Manuscript title: Characterisation of the multi-scale fabric features of high plasticity clays

Authors: F. Cotecchia*, S. Guglielmi*, F. Cafaro* and A. Gens†

Affiliations: *Department of Civil, Environmental, Land, Building Engineering and Chemistry, Politecnico di Bari, Bari, Italy and †Departamento de Ingeniería del Terreno, Universitat Politécnica de Catalunya, Barcelona, Spain

Corresponding author: S. Guglielmi, Department of Civil, Environmental, Land, Building Engineering and Chemistry, Politecnico di Bari, Via Edoardo Orabona, 4, 70126 Bari (BA), Italy. Tel.: +39 080 5963363.

E-mail: simona.guglielmi@poliba.it

Accepted manuscript doi:
10.1680/jgele.18.00230

Abstract

The letter describes an investigation of the microstructural features of a high-plasticity clay, in both its natural conditions and reconstituted in the laboratory. Scanning electron microscopy is used here to characterise the fabric at different magnification, while image processing of the micrographs delivers a quantitative assessment of the fabric orientation. Results of Energy dispersive X-ray spectroscopy and swelling tests, as reported in previous work by the authors, are used to characterise the bonding nature and strength, as well as mercury intrusion porosimetry to investigate the clay porosimetry. Despite their identical composition, the natural and the reconstituted clay have experienced different deposition and loading history, generating different microstructural features that are shown to underlie their differences in state. For both clays, 1D compression to medium-high pressures is seen to determine a well oriented medium magnification fabric. However, larger scale observations and the corresponding image processing results reveal non-uniform local fabric features, hence making fabric characterisation dependent on the scale of analysis and bringing about the issue of identifying the clay micro-scale representative element volume relating to the clay macro-behaviour. The micro-REV is identified for the clays under study and its connection with the macro-behaviour characterized. The microstructural evolution induced by 1D compression to very high pressures is shown to concern mainly the clay porosity and porosimetry, the fabric orientation being steady, thus explaining the isotropic hardening observed in laboratory tests.

Keywords: clays; fabric/structure of soils; microscopy

Accepted manuscript doi:
10.1680/jgele.18.00230

1. Introduction

The present letter discusses the microstructural features that a high plasticity natural clay achieves through its geological history, after one-dimensional (1D) compression in the laboratory (lab), and when reconstituted and subjected to 1D compression (Burland, 1990). The microstructure at the different macro-states: void ratio, e - vertical effective stress, σ'_v, is herein investigated making use of the scanning electron microscope (SEM) and the image processing of the micrographs at different magnifications. Results of Energy Dispersive X-ray Spectroscopy (EDS) in the SEM, mercury intrusion porosimetry (MIP) and, for the bonding strength, swelling tests (Schmertmann, 1969), reported in previous work, are also recalled.

The research results are aimed at characterizing the micro-scale sources of clay macro-behavioural features (e.g. Delage and Lefebvre, 1984; Hattab et al., 2013; Lima et al, 2008), traditionally modelled through the calibration of macro-mechanics models. Furthermore, they provide evidence of the complex processes taking place at colloidal scale, which should be modelled within micro-mechanical models of clays (e.g. Ebrahimi et al., 2012 and 2014, Anandarajah, 2000; Yao and Anandarajah, 2003, Ebrahimi et al., 2016; Liu et al., 2015; Sjoblom, 2016).

2. Composition, history and macro-behaviour of the clay

The investigated natural clay is the stiff Pappadai clay, deposited in the early Pleistocene in a quiet marine environment, within reducing conditions. The mineralogy and the index properties of the clay are reported in Table 1. It is mainly illitic, but includes a significant amount of smectite, interstratified illite-smectite and carbonatic silt. The Total Dissolved Solids (TDS) content and electrical conductivity of the squeezed pore fluid in the natural clay at Montemesola, in the same geological basin as Pappadai clay, allow to recognize a low salinity pore water (Fidelibus et al., 2018).

The history and the macro-behaviour of both the natural and the reconstituted Pappadai clay are discussed by Cotecchia & Chandler (1995 and 1997). Few macro-behaviour aspects, relating to the clay micro-scale processes, are recalled here.

The state of the natural clay, A in the compression plane in Figure 1, results from overconsolidation due to unloading (OCR= σ'_p/σ'_{v0} = 3; Cotecchia & Chandler 1995). When subjected to 1D compression in the lab (Figure 1), the clay exhibits gross yield at σ'_y about twice σ'_p (yield stress ratio, YSR=$\sigma'_y/\sigma'_{v0} \cong 2 \cdot$OCR) as result of diagenesis under burial, which has increased the strength of the clay bonding.

Following Burland (1990), the reconstituted Pappadai clay (parameters*), i.e. the clay achieving its microstructure through a lab history common for all reconstituted clays, was prepared as clay slurry of water content 1.25·LL. Given the low salt concentration in the pore fluid (Fidelibus et al., 2018) of the natural clay, distilled water was used to prepare the corresponding reconstituted clay slurry. Distilled water was also used to preserve saturation of both the natural and the reconstituted clay specimens during the mechanical tests. Its 1D compression curve plots to the left of the gross yield states of the natural clay (Figure 1).

The natural clay swell sensitivity, i.e. C_s^*/ C_{si} = 2.5 (Schmertmann, 1969), confirms the higher strength of the natural clay bonding with respect to that of the reconstituted, partly due to diagenesis. On the whole, the natural microstructure provides the clay with a stress sensitivity S_σ, σ'_y/σ^*_e ($\cong p'_{yis}/p^*_{yis}$ in isotropic compression; Cotecchia and Chandler, 2000) equal to 3.5 (Figure 1). Upon compression, the swell sensitivity of the natural clay drops to 1 soon after gross yield ($C_s^*/C_{s,py}$, Figure 1), but S_σ decreases gradually, as function of the plastic volumetric strain, ε_v^p, keeping a value above 1 up to high pressures.

Accepted manuscript doi:
10.1680/jgele.18.00230

The clay microstructure is an internal variable of the hardening function in several constitutive laws (e.g. Rouainia & Wood, 2000; Baudet & Stallebrass 2004). Cotecchia & Chandler (2000) showed that $S_\sigma(\varepsilon_v^p)$ is suited to represent its effects on the clay gross yield hardening, since the state boundary surface of several clays is normalized by the function $S_\sigma(\varepsilon_v^p)\cdot p_e^*(e)$ (p_e^* on the normal-consolidation line of the reconstituted clay; Schofield & Wroth 1968). Accordingly, an isotropic volumetric gross yield hardening function matches the large strain behaviour of several clays, either natural, or reconstituted, as shown for Pappadai clay in Figure 2.

3. Microstructure of the natural and the reconstituted clay

3.1 Testing procedures

Micrographs were achieved for vertical fractures of freeze-dried clay specimens, by means of SEM (gold coated) and Field Emission SEM (FESEM, carbon coated), as discussed by Cotecchia & Chandler (1998), Cotecchia et al. (2016) and Guglielmi et al. (2018). Digital image processing of the micrographs was carried out through an operator-independent technique, discussed for clays by Martinez-Nistal et al. (1999) and Mitaritonna et al. (2014). It is based on the thinning of the elongated bright regions across the micrograph, which represent either the edges of single particles, or the contour of oriented particle aggregates; an example of the thinning procedure is shown in Figure 3a. The thinning results in a field of vectors of varying orientation, processed to derive both a histogram of the detected orientations and a scalar "index of fabric orientation", L (e.g. Figure 3b). For a medium oriented fabric, L is about 0.21; L rises with increasing orientation, reaching 1 for a complete preferred orientation, c.p.o., fabric (Smart, 1969; Sides and Barden, 1970), whereas it is lower than 0.15 for "randomly oriented fabric" (Martinez-Nistal et al., 1999). The SEM micrographs and image processing data are discussed first for specimens pre-consolidated to medium-high pressures, i.e. states A* and A in Figure 1, and afterwards for those compressed to higher pressures, i.e. states B, C and C* in the figure.

EDS was used in the A state investigation (Cotecchia and Chandler, 1997). MIP tests were carried out on the clay (Guglielmi et al., 2018) at states A, B and C (Figure 1).

3.2 Microstructural features of the clay compressed to medium-high pressures

The reconstituted clay reaches state A* (e=1.28 - σ'_v=20 kPa; Figure 1) through swelling from σ'_p*=200 kPa. Figure 4a shows a micrograph exemplifying the A* clay fabric on vertical fractures of about 10^4 μm^2 size area (cubic volume 10^{-3} mm^3), investigated at 10^3 magnification, defined as 'medium scale' (Collins and McGown, 1974; O'Brien and Slatt, 1990). At such scale, the fabric is found to match a repetitive pattern, formed of densely packed domains (Figure 4c) in face to face contact, forming stacks (Sides and Barden, 1970; Figures 4b and c), locally confining either macro-pores (i.e. diameter above 1 μm; Matsuo and Kamon, 1977; Guglielmi et al., 2018), or aggregates of randomly oriented particles/domains, in edge to face contact (Figures 4b and c). The image processing of several medium magnification micrographs of the A* clay has delivered L values varying in a narrow range, 0.23-0.27 (e.g. Figure 4d). Hence, the fabric pattern repeatedly detected at medium scale, is generally characterized by a medium-good orientation (Martinez-Nistal et al. 1999). A repetitive porosimetry is expected to correspond to such fabric pattern.

Also for the overconsolidated natural diagenized clay, at state A (e=0.88 - σ'_v=414 kPa; Figure 1), both the qualitative analysis and the image processing of several medium scale micrographs has resulted in the recognition of a repetitive fabric. Also this is formed by a dense packing of stacks, locally burying either randomly oriented domains (e.g. bookhouse, Figures 4c and 5b), or macropores, or micro-fossils (Cotecchia and Chandler, 1998). The

Accepted manuscript doi:
10.1680/jgele.18.00230

direction histograms resulting from the image processing (e.g. Figure 5c) deliver L in the range 0.24-0.37, indicative of a good orientation fabric. The MIP test results for state A show that the clay pore size distribution is mainly monomodal, with dominant pore size in the range of micro-porosity and a well distributed macro-porosity (Guglielmi et al., 2018). Therefore, the micro-investigation results show that, irrespective of the differences in history, both the natural and the reconstituted clay have achieved, through 1D pre-consolidation to medium-high pressures, a medium-scale fabric characterized by a medium to good orientation.

At higher magnifications (i.e. 10^4-10^5; clay portions of about 10^{-6} mm^3 volume; 'large' scale hereafter), in either the A* reconstituted, or the A natural clay, the local fabric is highly variable, going from a c.p.o. (Figures 6a and b) to a randomly oriented fabric (Figures 6c and d). For both the clays, the image processing at the large scale results in variable indices of orientation, $0.15<L<0.28$, accordingly (Figure 6). Such variability in local fabric is likely to apply to other natural and reconstituted clays 1D pre-consolidated to medium-high pressures; as such it gives evidence to the general need of characterizing the micro-scale representative element volume of the clay, micro-REV, in order to assess the micro-scale features of the clay. By definition, the micro-REV fabric must include, in a repetitive way, the different local fabric features, according to their frequency, so as to fulfil the role of internal variable controlling the clay macro-behaviour.

For the clays under study, the micro-REV size is necessarily higher than 10^{-6} mm^3, which is investigated at large-scale (Figure 6). Rather, the clay micro-REV corresponds to the clay portion, of size about 10^{-3} mm^3, investigated at the medium-scale and found to be characterized by a repetitive fabric and L value. Given so, the data show that by medium preconsolidation pressures the micro-REV of the reconstituted Pappadai clay achieves a degree of orientation only slightly lower than that of the natural clay preconsolidated to a σ'_p about 5 times higher. At the same time, the micro-REV structures of the clays at A and A* differ for: i) the stronger bonding of the A natural clay ($C_s^*/C_{si} = 2.5$), which is partly effect of an amorphous calcite film binding the natural clay particles, effect of diagenesis and detected through EDS (Cotecchia & Chandler 1997); ii) the higher size and quantity of the macro-pores in the A* clay state; iii) a rather more chaotic fabric within the 'randomly oriented fabric' portions locally occurring in the natural clay.

3.3 Microstructural features of the clay compressed to higher pressures

Figure 7a shows a medium-magnification micrograph of the reconstituted clay 1D compressed to σ'_v=22 MPa (state C*, Figure 1). With respect to the micro-REV fabric at A*, at C* the fabric packing is far denser, the macro-pores are much fewer and the layers of piled stacks thicker. Nonetheless, the average degree of orientation at C* is about that at A*, since L values about 0.24 are recorded. Mitaritonna et al. (2014) reported a similar finding for the illitic reconstituted Lucera clay, shown to have a medium-scale L (=0.28) constant in 1D ($\eta=q/p'=0.6$) compression from σ'_v=140 kPa to 1900 kPa. It follows that the orientation of the micro-REV fabric does not increase in 1D compression from medium to very high pressures, differently from what assumed in the literature (e.g. Morgenstern and Tchalenko, 1967; Tchalenko, 1967; Delage and Lefebvre, 1984; Lapierre et al., 1990; Hicher et al., 2000; Hattab et al., 2013). Furthermore, at C*, the same as at A*, the fabric within the micro-REV is still not uniform, as evident at large scale (example of local randomly oriented fabric in Figure 7b).

Mitaritonna et al. (2014) showed also that, in constant η compression, a constancy in elastic stiffness anisotropy corresponds to the constant medium-scale degree of fabric orientation. Conversely, such anisotropy varies when the medium-scale fabric achieves a different

orientation index, L, after a significant compression at a different η. This finding suggests that the clay macro-behaviour at very small strains relates with the medium-scale clay fabric features, here recognized to be the clay micro-REV fabric.

The micro-investigation data discussed above for reconstituted Pappadai clay show that also the clay hardening law relates with the clay micro-REV fabric features. The finding that, in 1D compression to very high pressures, the changes in micro-REV fabric concern mainly the clay porosity and porosimetry, but not the index of orientation, is consistent with the isotropic volumetric hardening function fitting the large-strain macro-behaviour of reconstituted clays (e.g. Schofield and Wroth 1968; Roscoe and Burland, 1968; Figure 2). Hence, the clay micro-REV fabric, characterized at the medium scale, is confirmed to be an appropriate internal variable of the clay macro-behaviour.

For the natural clay, gross yielding is observed to cause major weakening of the natural bonding, given the drop in C_s^*/C_s recorded between states A and B (soon after gross yield). Figure 8a shows one of several medium scale micrographs for state B, which suggest that gross yielding causes also some fabric rearrangement, e.g. the chaotic filling of macro-pores with particle aggregates. However, the micro-REV fabric does not attain a higher orientation degree, as confirmed by the L value (Figure 8a).

With post-gross yield compression to state C (σ'_v=25 MPa), the natural micro-REV fabric (Figure 9a) is repeatedly formed by thickened layers of c.p.o. fabric, interbedding randomly oriented fabric portions, as recognized through large scale micro-investigation (Figures 9c and d). Therefore, the micro-REV fabric is not uniform even in the natural clay at very high pressures and 1D compression determines either the piling up of stacks in extremely low porosity layers, or the shift of randomly oriented aggregates (e.g. Figs. 8b and 9c), which do not necessarily collapse under very high pressures. MIP testing shows that, while the clay macro-porosity becomes negligible by state B, a progressive reduction of the dominant pore size is attained all way through compression (Guglielmi et al., 2018). In the meanwhile, the micro-REV fabric does not achieve a much higher degree of orientation, since values of L in the range $0.24<L<0.345$, are recorded.

Such constancy in micro-REV fabric orientation is consistent with the isotropic volumetric gross yield hardening law fitting the natural clay macro-scale behaviour (Figure 2), $S_\sigma(\varepsilon_v^p)\cdot p_e^*(e)$ (Cotecchia & Chandler 2000). This accounts for a positive hardening conferred by the positive volumetric straining, and, through $S_\sigma(\varepsilon_v^p)$, for the negative hardening conferred by the weakening of the clay structure.

4. Conclusions

The paper highlights that the fabric is not uniform in clays 1D compressed from medium to very high pressures. Hence, it is necessary to identify the micro-REV fabric that, for the clays under study, has 10^{-3} mm^3 volume. This is characterized through the image processing of 10^3 magnification micrographs and has been shown to relate with the clay macro-response, at both small and large strains.

Furthermore, the letter reveals that, for both the natural and the reconstituted clay, the micro-REV fabric orientation is medium to good by medium pressures and does not increase much during constant η compression to very high pressures. The isotropic volumetric gross yield hardening of the clay is an effect of such micro-REV structure evolution with compression. At large scale, compression determines either the coalescence of stacks, or the shift of randomly oriented fabric portions, which do not necessarily undergo collapse.

Acknowledgements
The authors thank Dr. Vito Summa and Dr. Antonio Lettino of the Institute of Methodologies for Environmental Analysis (IMAA) of the National Research Council (CNR) at Tito Scalo (PZ, Italy) for the use of the FESEM. They are also grateful to Dr. Angel Martinez-Nistal for the image processing of the micrographs.
The authors express their gratitude to Fondazione Puglia for supporting the research.

List of notation

A	clay activity
CF	clay fraction
CRS	constant rate of strain oedometer test
C_s	swelling index
C_s^*/C_s	swell sensitivity
e	void ratio
L	index of fabric orientation
OCR	overconsolidation ratio: σ'_p/σ'_v
OED	conventional oedometer test
PI	plasticity index
S_σ	Stress Sensitivity
w	water content
YSR	yield stress ratio: σ'_y/σ'_v
σ^*_e	equivalent vertical effective stress on the ICL
σ'_p	vertical (geological) preconsolidation pressure
σ'_v	vertical effective stress
σ'_y	vertical effective stress at yield

References

Anandarajah A (2000) Numerical simulation of one-dimensional behaviour of a kaolinite. Géotechnique **50(5)**: 509–519.

Baudet BA and Stallebrass SE (2004) A constitutive model for structured clays. Géotechnique **54**: 269-278.

Burland J.B. (1990) On the compressibility and shear strength of natural soils. Géotechnique **40 (3)**: 329-378.

Collins K and McGown A (1974) The form and function of microfabric features in a variety of natural soils Géotechnique **24 (2):** 223-254.

Cotecchia F and Chandler RJ (1995) The geotechnical properties of the Pleistocene clays of the Pappadai valley. Quarterly Journal of Engineering Geology **28**: 5-22.

Cotecchia F and Chandler RJ (1997) The influence of structure on the pre-failure behaviour of a natural clay. Géotechnique **47 (3)**: 523-544.

Cotecchia F and Chandler RJ (1998) One-dimensional compression of a natural clay: structural changes and mechanical effects. In *Proceedings of the 2nd International Symposium on Hard Soils Soft Rocks*, 103-114.

Cotecchia F and Chandler RJ (2000) A general framework for the mechanical behaviour of clays. Géotechnique **50**: 431-447.

Cotecchia F, Cafaro F, Guglielmi S (2016) Microstructural changes in clays generated by compression explored by means of SEM and Image Processing. Procedia Engineering **158**: 57-62.

Delage P and Lefebvre G (1984) Study of the structure of a sensitive Champlain clay and of its evolution during consolidation. Canadian Geotechnical Journal **21 (1)**: 21-35.

Ebrahimi D, Pellenq RJ-M, Whittle AJ (2012) Nanoscale elastic properties of montmorillonite upon water adsorption. Langmuir **28 (49)**: 16855–16863.

Ebrahimi D, Whittle AJ, Pellenq RJ-M (2014) Mesoscale properties of clay aggregates from potential of mean force representation of interactions between nanoplatelets. The Journal of Chemical Physics **140 (15)**: 154309.

Ebrahimi D, Pellenq RJ-M, Whittle AJ (2016) Mesoscale simulation of clay aggregate formation and mechanical properties. Granular Matter **18 (3)**: 1–8.

Fidelibus MD, Argentiero I, Canora F, Pellicani R, Spilotro G, Vacca G (2018) Squeezed interstitial water and soil properties in Pleistocene Blue Clays under different natural environments. Geosciences 2018, **8**, 89; doi:10.3390/geosciences8030089.

Guglielmi S, Cotecchia F, Cafaro F, Gens A (2018) Microstructural changes underlying the macro-response of a stiff clay. P. Giovine et al. (eds.), Micro to MACRO Mathematical Modelling in Soil Mechanics, Trends in Mathematics, Springer Nature Switzerland AG 2018, pp.89-97.

Hattab M, Hammad T, Fleureau J-M, Hicher P-Y (2013) Behaviour of a sensitive marine sediment: microstructural investigation. Géotechnique **63 (1)**: 71- 84.

Hicher P-Y, Wahyudi H, Tessier D (2000) Microstructural analysis of inherent and induced anisotropy in clay. Mech. Cohes.-Frict. Mater. **5**: 341-371.

Lapierre C, Leroueil S, Locat J (1990) Mercury intrusion and permeability of Louiseville clay. Can. Geotech. J. **27**: 761-773.

Lima A, Romero E, Pineda JA, Gens A (2008) Low-strain shear modulus dependence on water content of a natural stiff clay. In *Proceedings of XIV Congresso Brasileiro de Mecanica dos Solos e Engenharia Geotécnica*, 1763-1768.

Liu J, Lin CL, Miller JD (2015) Simulation of cluster formation from kaolinite suspensions. International Journal of Mineral Processing **145**: 38–47.

Martinez-Nistal A, Vinale F, Setti M, Cotecchia F (1999) A scanning electron microscopy image processing method for quantifying fabric orientation of clay geomaterials. Applied Clay Science **14**: 235-243.

Matsuo S and Kamon M (1977) Microscopic study on deformation and strength of clays, Proceedings of the 9th ICSMFE, Tokyo, **1**: 201-204

Mitaritonna G, Amorosi A, Cotecchia F (2014) Experimental investigation of the evolution of elastic stiffness anisotropy in a clayey soil. Géotechnique **64 (6)**: 463-475.

Morgenstern NR and Tchalenko JS (1967) Microscopic structures in kaolin subjected to direct shear. Géotechnique **17**: 309-328.

O'Brien NR and Slatt RM (1990) *Argillaceous Rock Atlas*, Springer-Verlag, Berlin.

Accepted manuscript doi:
10.1680/jgele.18.00230

Roscoe KH and Burland JB (1968) On the generalized stress-strain behaviour of wet clay, In Engineering Plasticity (J. Heymann and F.A. Leckie, eds), Cambridge University Press, Cambridge, pp. 535-609.

Rouainia M and Muir Wood D (2000) A kinematic hardening constitutive model for natural clays with loss of structure. Géotechnique **50 (2)**: 315-321.

Schmertmann JH (1969) Swell sensitivity. Géotechnique **19**: 530-533.

Schofield AN and Wroth CP (1968) *Critical State Soil Mechanics*, Mc Graw-Hill Book Co., London.

Sides G and Barden L (1970) The microstructure of dispersed and flocculated samples of kaolinite, illite and montmorillonite. Canadian Geotechnical Journal **8**: 391-399.

Sjoblom KJ (2016) Coarse-Grained Molecular Dynamics Approach to Simulating Clay Behavior. Journal of Geotechnical and Geoenvironmental Engineering ASCE **142 (2)**: 1–6.

Smart P (1969) Soil structure in the electron microscope. Proc. Int. Conf. Structure. Solid Mech. Eng. Des. Civil Eng. Mater., University of Southampton, Southampton, England.

Tchalenko JS (1967) The influence of shear and consolidation on the microscopic structure of some clays. PhD thesis, London University.

Yao M and Anandarajah A (2003) Three-Dimensional Discrete Element Method of Analysis of Clays. ASCE Journal of Engineering Mechanics **129 (6)**: 585–596.

Table captions

Table 1. Index properties, mineralogy and initial state of natural Pappadai clay (after Cotecchia and Chandler, 1997).

Accepted manuscript doi:
10.1680/jgele.18.00230

Table 1. Index properties, mineralogy and initial state of natural Pappadai clay (after Cotecchia and Chandler, 1997).

Composition and physical properties	Specific gravity, G_s	2.75
	Clay fraction, CF	58%
	Silt fraction, MF	41%
	Sand fraction, SF	1%
	Liquid limit. LL	65%
	Plasticity index, PI	35%
	Activity, A	0.6
	Natural water content, w_0	≈31%
	In situ void ratio, e_0	0.88
	Carbonate content	28%
Mineralogy	Quartz	3%
	Feldspar	1%
	Carbonate	22%
	Dolomite	6%
	Kaolinite	12%
	Chlorite	14%
	Illite	20%
	Smectite	12%
	Interstratified	10%
	Total	100%

Accepted manuscript doi:
10.1680/jgele.18.00230

Figure captions

Figure 1. One-dimensional compression and swelling tests on both natural and reconstituted (*) Pappadai clay (adapted from Cotecchia and Chandler, 1997).

Figure 2. Pappadai clay: gross yield data of the natural clay and stress paths of the reconstituted clay, behaviour normalized for both volume and structure (after Cotecchia and Chandler, 2000).

Figure 3. Natural Pappadai clay, A (Fig.1): a) FESEM with processed overlay and b) corresponding direction histogram and index of fabric orientation.

Figure 4. Reconstituted Pappadai clay, A* (Fig.1): a) medium magnification micrograph (after Cotecchia et al., 2016) with b) examples of different local fabric arrangements; c) classification of fabrics (after Sides and Barden, 1970, modified); d) direction histogram and index of fabric orientation of micrograph 4a (after Cotecchia et al., 2016).

Figure 5. Natural Pappadai clay, A (Fig.1): a) medium magnification micrograph with b) examples of different local fabric arrangements; c) corresponding direction histogram and index of fabric orientation (after Cotecchia et al., 2016).

Figure 6. High magnification micrographs of Pappadai clay, with examples of different local fabric arrangements (i.e. complete preferred orientation, c.p.o., and randomly oriented fabric), and corresponding indices of fabric orientation. a) and c), reconstituted clay (state A*, Fig.1); b) and d), natural clay (state A, Fig.1).

Figure 7. Compressed reconstituted Pappadai clay, C* (Fig.1): a) medium magnification micrograph (with examples of different local fabric arrangements) and index of fabric orientation; b) high magnification micrograph and index of fabric orientation.

Figure 8. Compressed natural Pappadai clay, B (Fig.1): a) medium magnification micrograph (with examples of different local fabric arrangements; after Cotecchia et al., 2016 modified) and index of fabric orientation; b) high magnification micrograph and index of fabric orientation.

Figure 9. Compressed natural Pappadai clay, C (Fig.1): a) medium magnification micrograph (with examples of different local fabric arrangements) and b) corresponding direction histogram and index of fabric orientation; c) and d) higher magnification micrographs and indices of fabric orientation, indicative of the variability in fabric arrangement.

Accepted manuscript doi:
10.1680/jgele.18.00230

Figure 1

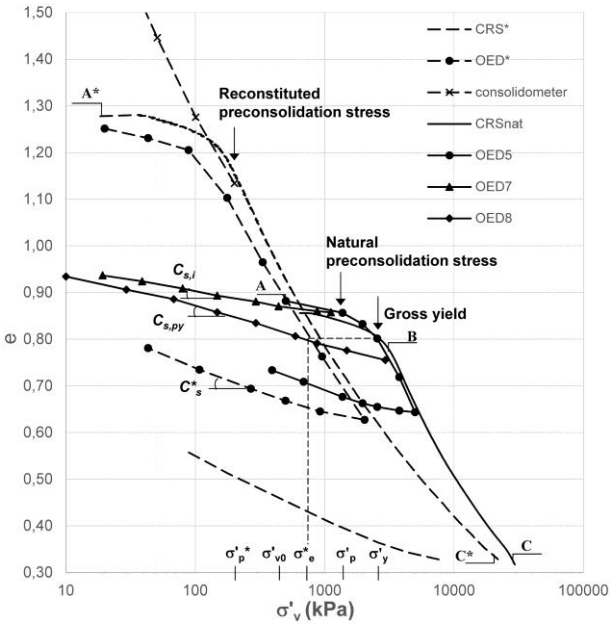

Accepted manuscript doi:
10.1680/jgele.18.00230

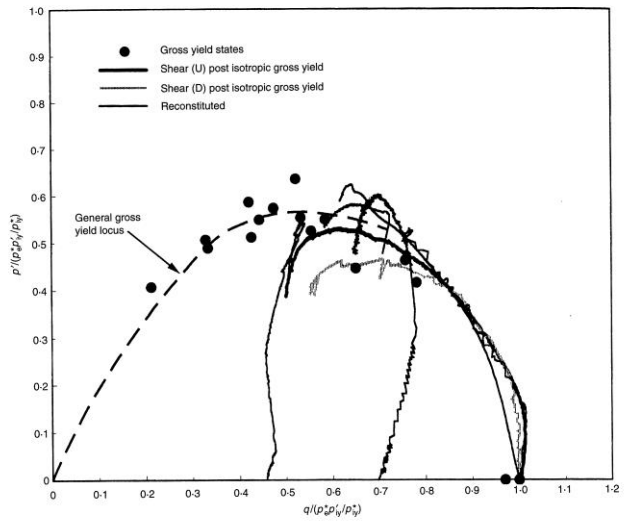

Figure 2

Accepted manuscript doi:
10.1680/jgele.18.00230

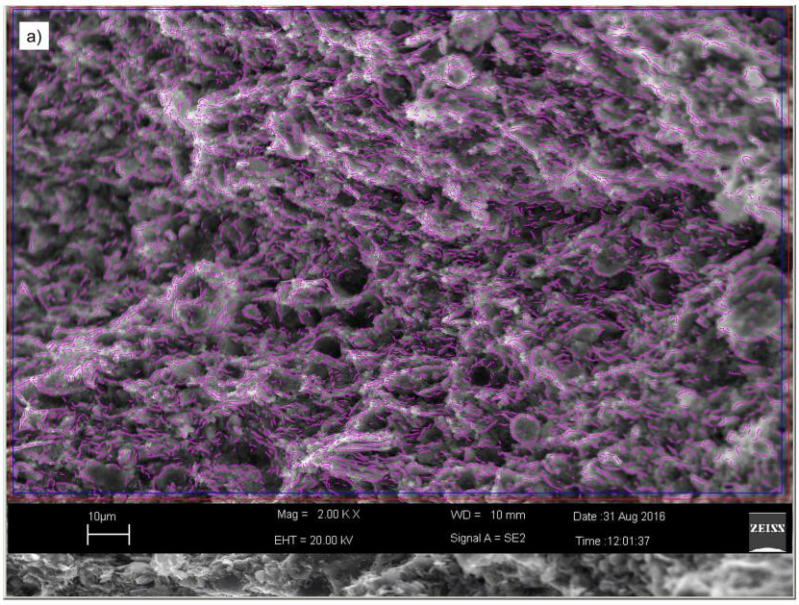

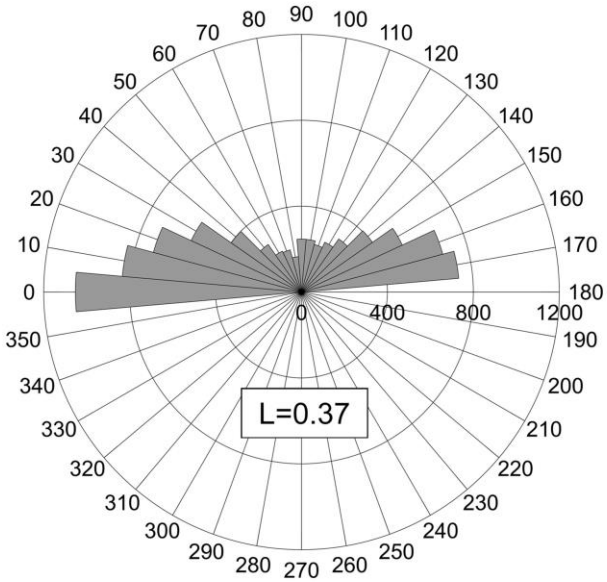

Figure 3

b

Accepted manuscript doi:
10.1680/jgele.18.00230

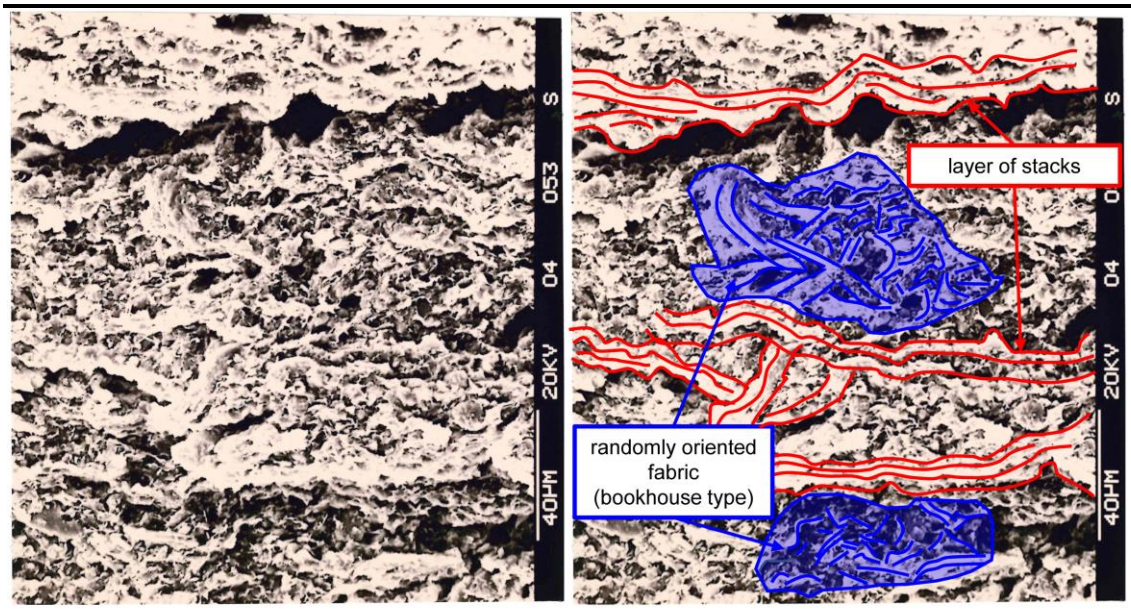

a) b)

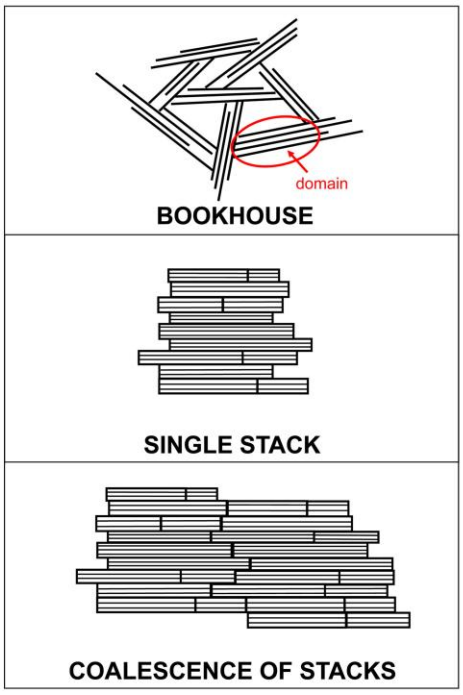

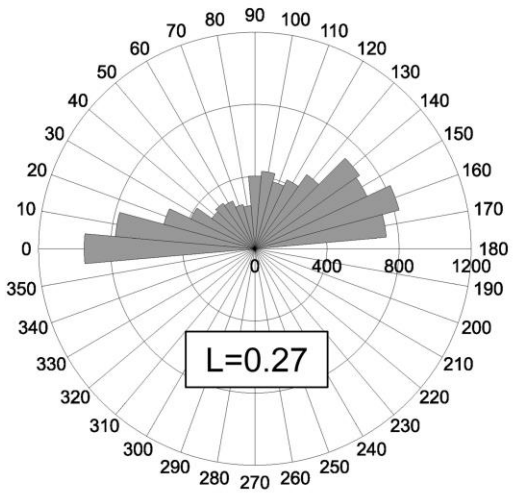

c) d)

Figure 4

Accepted manuscript doi:
10.1680/jgele.18.00230

Figure 5

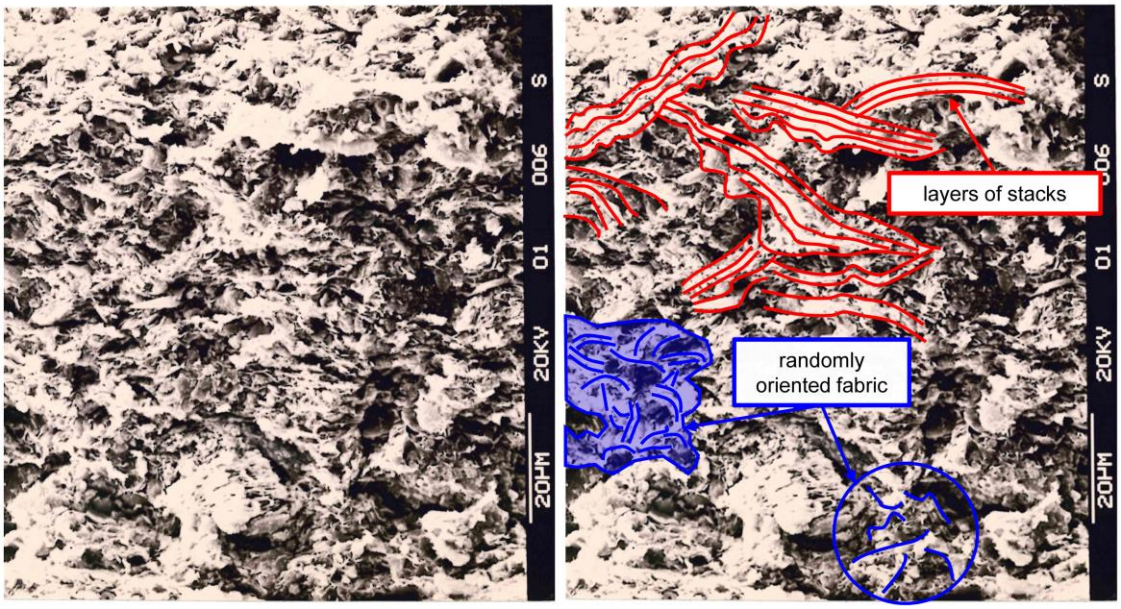

a) b)

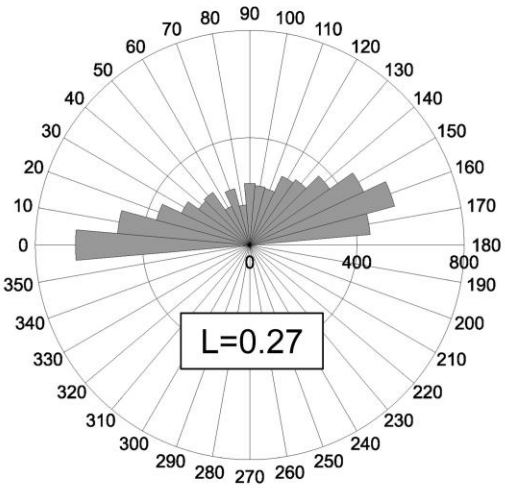

c)

Accepted manuscript doi:
10.1680/jgele.18.00230

Figure 6

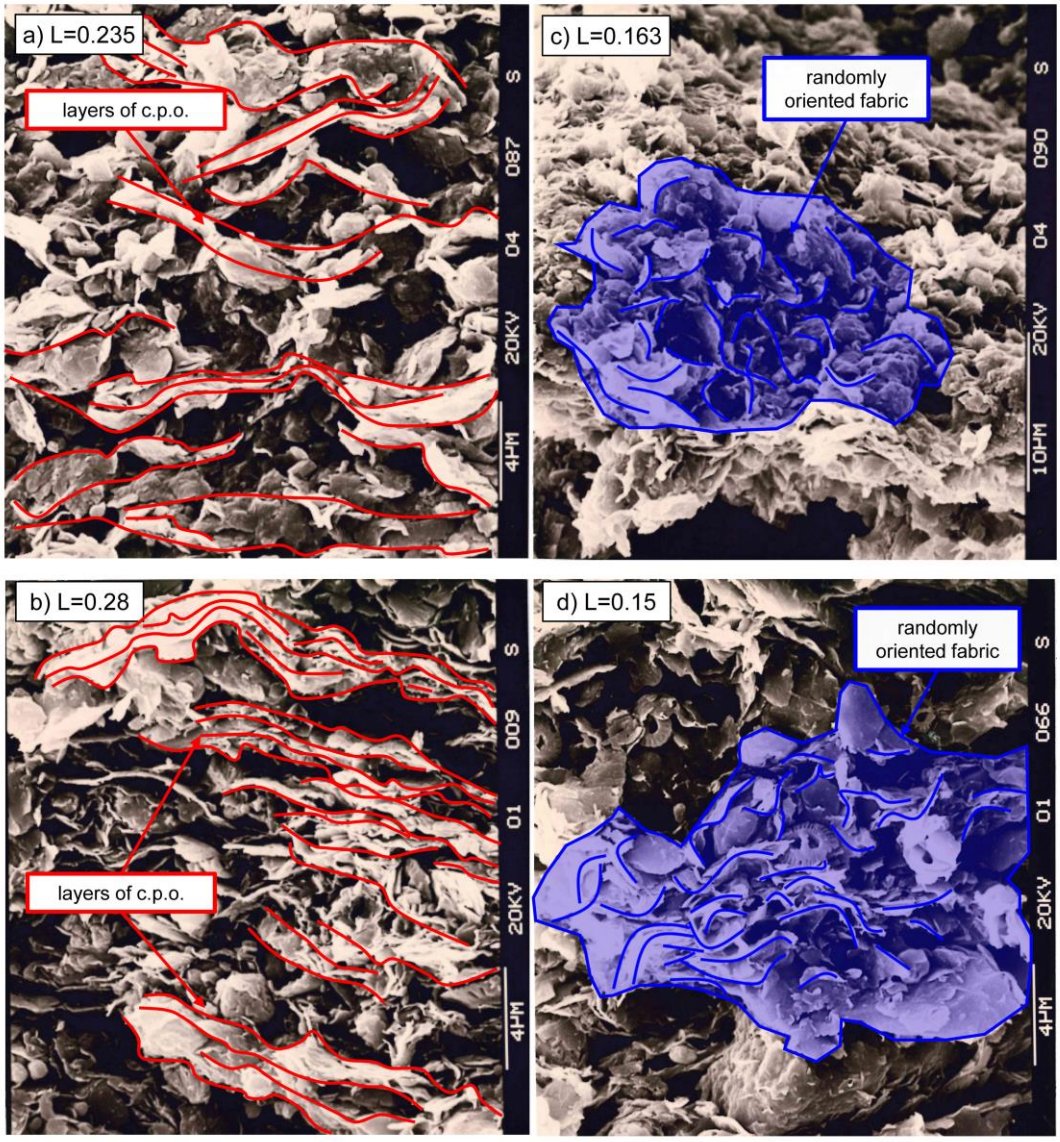

Accepted manuscript doi:
10.1680/jgele.18.00230

Figure 7

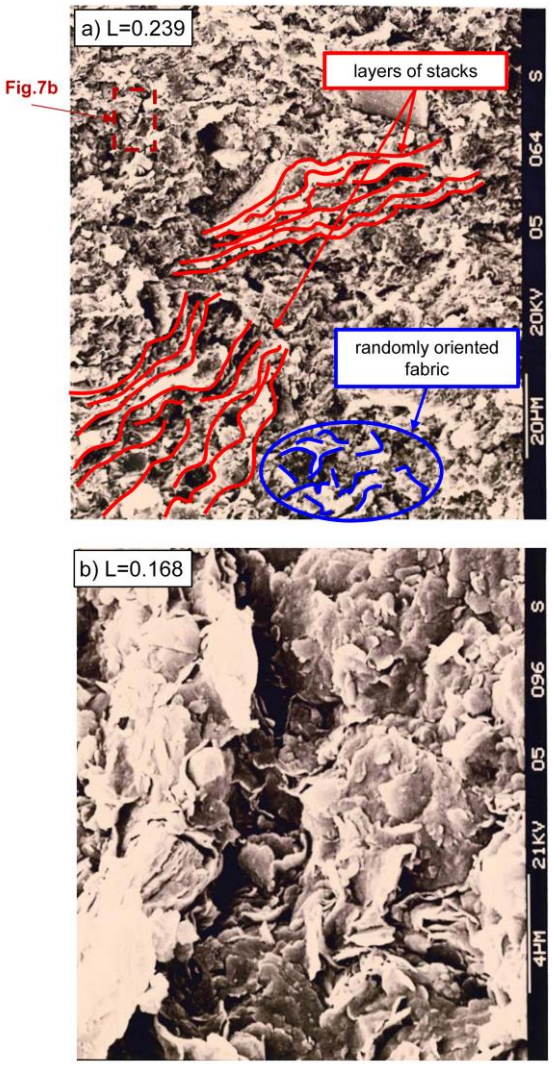

Accepted manuscript doi:
10.1680/jgele.18.00230

Figure 8

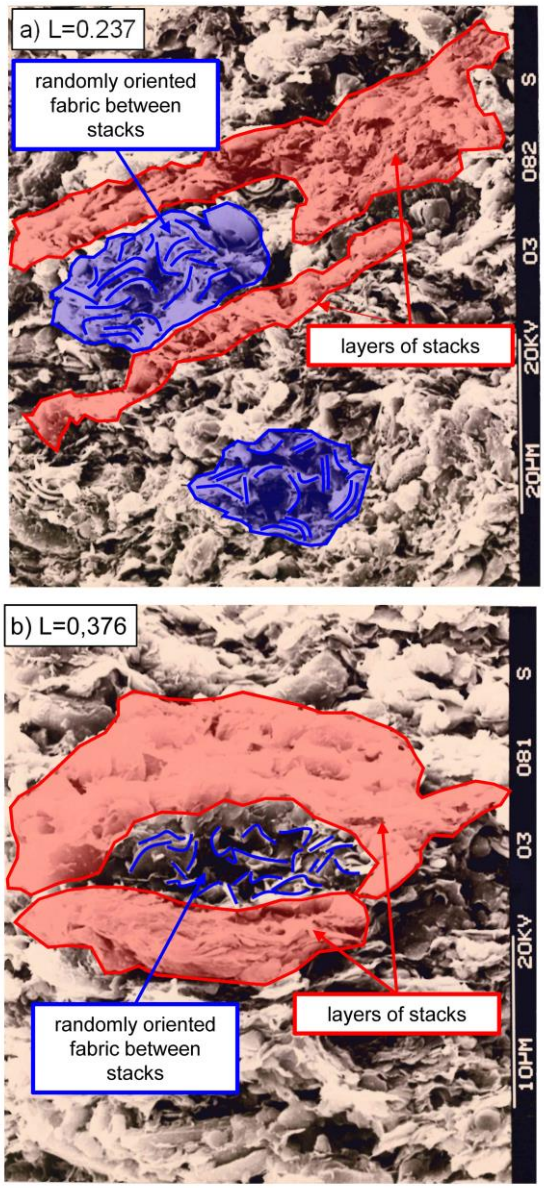

Accepted manuscript doi:
10.1680/jgele.18.00230

Figure 9

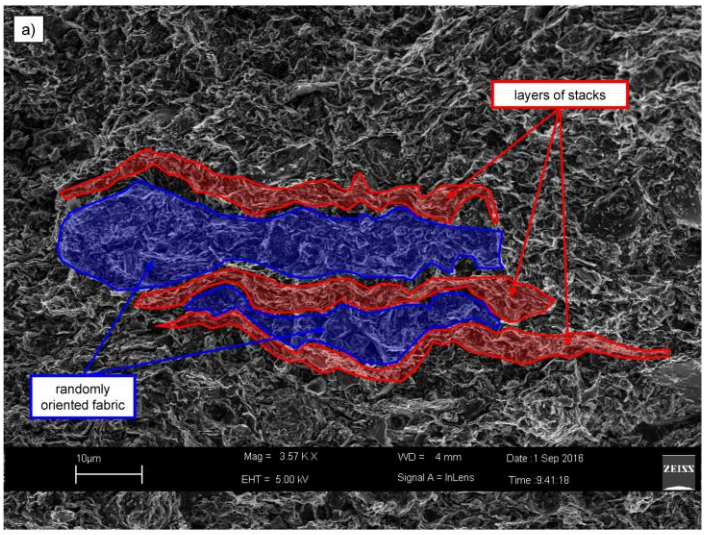

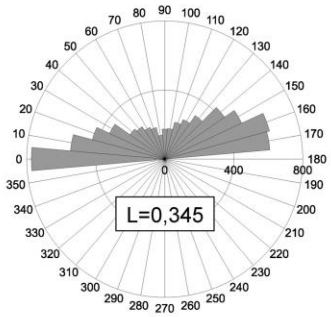

b)